CHALMERS

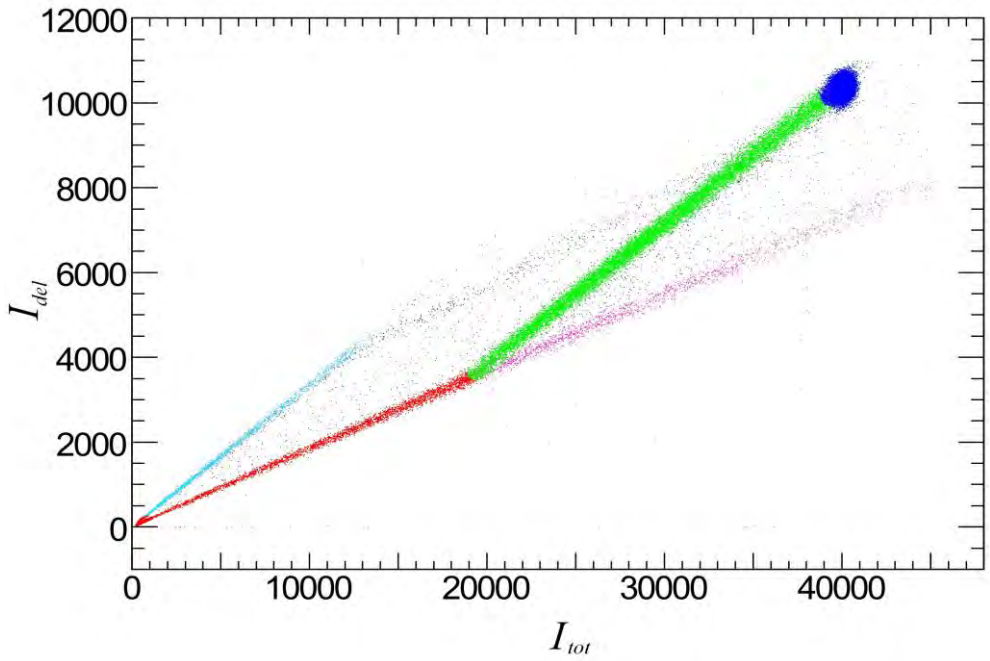

Proton beam test of CALIFA detector prototypes

Bachelor Thesis in Engineering Physics

BERGSTRÖM, JOHAN M.R.
BLOMBERG, ERIK M.
GALLNEBY, ERIK A.
HAGDAHL, JULIUS E.
NORDSTRÖM, MARTIN O.
WITTLER, HENRY P.A.

Department of Fundamental Physics
Subatomic Physics Group
CHALMERS UNIVERSITY OF TECHNOLOGY
Göteborg, Sweden, 2009

Chalmers University of Technology
Engineering physics
Göteborg

Department of Fundamental Physics
Subatomic physics group
Thomas Nilsson

Proton beam test of CALIFA detector prototypes

BACHELOR THESIS

Bergström, Johan M.R.
bergstrj@student.chalmers.se

Blomberg, Erik M.
blombere@student.chalmers.se

Gallneby, Erik A.
gallneby@student.chalmers.se

Hagdahl, Julius E.
juliush@student.chalmers.se

Nordström, Martin O.
martno@student.chalmers.se

Wittler, Henry P.A.
guswitth@student.gu.se

31st May 2009

Abstract

A variety of detector prototypes proposed for the CALIFA calorimeter at the planned FAIR facility in Darmstadt, Germany, have been subjected to proton beam testing at TSL in Uppsala, Sweden. The prototypes tested were inorganic scintillators composed of single CsI(Tl) and $LaBr_3$(Ce) crystals, as well as a phoswich detector composed of a $LaBr_3$(Ce) and a $LaCl_3$(Ce) crystal.

A data acquisition system was designed and assembled for this experiment in order to provide accurate measurement data at a adequate rate. Acquired phoswich pulse data has been analysed using two different methods; one based on comparisons between pulse amplitudes and integrals, and one based on comparisons between integrals over different intervals.

Results from the phoswich data analysis show a clear separation of measurement data originating from different types of physical events. This, along with successful translation of relative amplitude measurements into deposited proton energies, indicates a good performance of the phoswich prototype in proton energy measurements.

Contents

Appendices

List of Figures

1 Introduction

An important subject of subatomic physics is the study of exotic, unstable nuclei using beams of radioactive ions. A large facility for research and development in this field, GSI (refer to the glossary on page 43 for explanations of terminology and abbreviations), is located in Darmstadt, Germany. An international cooperative project, FAIR, aims to extend and develop the existing particle accelerator facility. Figure 1 shows an overview of the existing GSI-facility and the planned FAIR extensions. Part of the planned FAIR-facility is the fixed target R^3B-setup, with the purpose of studying various properties of exotic nuclei. [1]

At R^3B a beam of exotic nuclei will collide with a target, releasing highly energetic neutrons, protons and gamma photons along with heavier fragments. These scattered particles provide important information regarding the properties of the incoming nuclei. A calorimeter, CALIFA, consisting of an array of scintillating crystal detectors surrounding the target will be used for energy measurements of scattered protons and emitted gamma reaction rays.

Particles scattered forward in the beam direction after colliding inside CALIFA will have much higher energies than particles scattered in larger angles with respect to the beam. Therefore, the required properties of the CALIFA detector crystals will vary significantly depending on their placement in the structure. Testing of different designs and materials for these detectors is an ongoing process. [2]

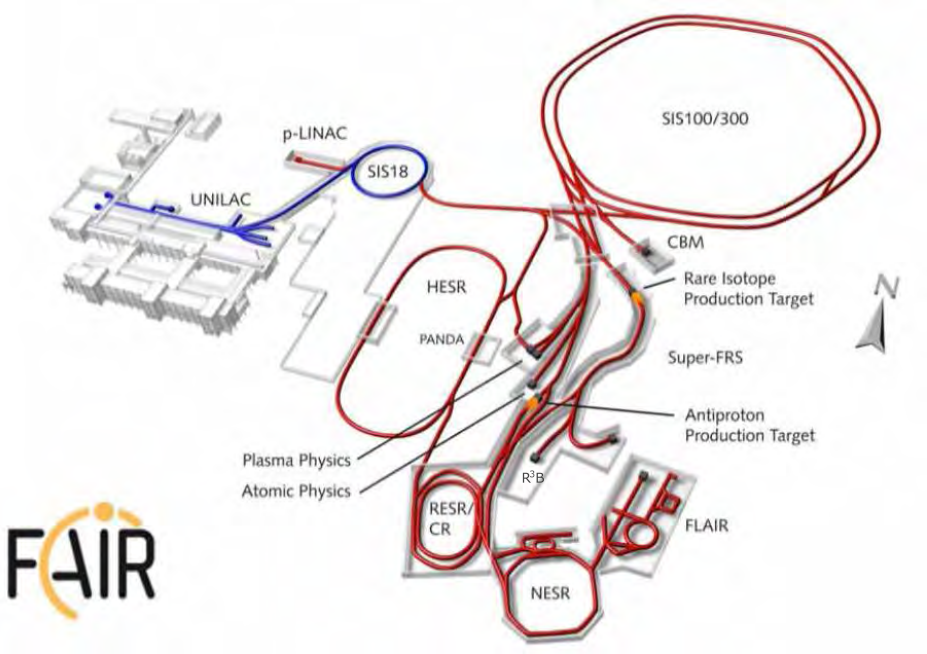

Figure 1: Overview of GSI, with the FAIR-additions drawn as they are planned to be built.

1.1 Purpose and scope

This report aims to describe the testing of CALIFA detector prototypes at the TSL experiment during March 2009. The two main concerns are the experiments' data acquisition system and the analysis of acquired data.

The DAQ system used in the prototype tests at TSL will be described, as well as the methods used for testing and debugging this system. Also provided is a "how to" on setting up such a system, including both general guidelines and an example with actual wiring schematics.

Analysis of the data acquired at TSL will focus on determining how, if at all, correct energy measurements can be extracted from the phoswich detector ADC and SADC data. The main challenge here is how to separate the combined pulse resulting from energy deposition in both of the phoswich's materials into two different components; one for each material.

2 Background and theory

The purpose of this section is to give an orienting background in the relevant fields of subatomic physics and radioactive decay of exotic nuclei, as well as introduce the R^3B experiment, explain scintillating detectors and cover relevant topics of data analysis.

2.1 Exotic nuclei

Most elements have more than one stable isotope; a stable helium nucleus can, for example, contain either one or two neutrons in addition to its two protons. These isotopes correspond to the most energy efficient configurations of the nuclei, within that particular isobar. [3]

In addition to these stable nuclear configurations there are isotopes with an excess or deficiency of neutrons. These nuclei will attempt to reach a lower energy state, a stable isotope, through radioactive decay. The lifetime of radioactive isotopes vary significantly, however exotic nuclei often have very short lifetime. Thus, to study these isotopes, one must generally create them artificially through collisions between other, stable, nuclei and particles. Due to the nature of exotic nuclei, they can display properties that make them substantially different from their stable counterparts. One example of this are halo nuclei, which have valence neutrons or protons that are very weakly bound. Therefore, instead of clustering with the other protons and neutrons in the usual way, they form a halo at a large distance outside the main nucleus. This gives a halo nucleus a very large radius compared to a stable nucleus of the same element, which is experimentally observed through, among other things, increased reaction cross-sections.

2.1.1 Radioactive decay

Unstable nuclei have highly varying life times before they spontaneously decay into more stable configurations, directly or in several steps. The unstable isotopes can be so short-lived that the formation state can never be observed; it may very well not even be a bound state. These isotopes can only be identifed by the fragments they leave behind as they fall apart. In the case of unstable, but bound, configurations, the isotope will instead decay radioactively. Radioactive decay of atoms can be divided into three main types; alpha- (α), beta- (β) and gamma- (γ) decay, which differ both in the acting fundamental forces and in the characteristic particles they emit.

α decay is a process governed by the strong nuclear force and electromagnetism. Through this process, a nucleus will decay into a lighter element by emitting an α particle, i.e., a ^{4}He-nucleus.

$$\alpha: \quad {}^{A}_{Z}X_N \rightarrow {}^{A-4}_{Z-2}X'_{N-2} + \alpha \tag{1}$$

β decay is governed by the weak interaction and comes in three different varieties; β^-, β^+ and electron capture (EC). During β^- and β^+ decay, a neutron decays into a proton, or vice versa. This is accompanied by the emission of an electron and an anti-neutrino or a positron and a neutrino respectively. Electron capture occurs when a nucleus interacts with an atomic electron, converting a neutron to a proton and emitting a neutrino. EC and β^+ decay can not happen to free protons and electrons, but only occur in bound nuclear states.

$$\beta^-: \quad {}^{A}_{Z}X_N \rightarrow {}^{A}_{Z+1}X'_{N-1} + e^- + \overline{\nu} \tag{2}$$

$$\beta^+: \quad {}^{A}_{Z}X_N \rightarrow {}^{A}_{Z-1}X'_{N+1} + e^+ + \nu \tag{3}$$

$$EC: \quad {}^{A}_{Z}X_N + e^- \rightarrow {}^{A}_{Z-1}X'_{N+1} + \nu \tag{4}$$

γ decay generally occurs as a side effect of α or a β decay. After these processes, the resulting nucleus can be left in an excited state and will have to emit the excess energy in the form of a γ photon to reach its ground state. Thus, this decay neither affects the atomic number nor the mass number of the decaying nucleus, as it is only a transition between different energy states of the same isotope.

$$\gamma: \quad {}^{A}_{Z}X_N{}^* \rightarrow {}^{A}_{Z}X_N + \gamma \tag{5}$$

Where X^* represents an excited nucleus. γ decay often occurs in several steps, where each step emits a photon with a characteristic energy.

2.2 R^{3}B experiment overview

The international R^{3}B collaboration aims to develop and construct a versatile experiment setup for measuring reactions with high-energy radioactive beams. For an overview of the experimental setup refer to figure 2. Important factors for consideration are efficiency, energy acceptance and resolution, as well as giving kinematically complete measurements, i.e., depositing all of the energy released in the collisions into detectors. [4]

2.2.1 Radioactive beam production

The radioactive beam at R^{3}B is produced in several steps. First, a beam of stable ions, known as the primary beam, is produced in the SIS100/300 synchrotrons. These ions are accelerated to relativistic velocities before colliding

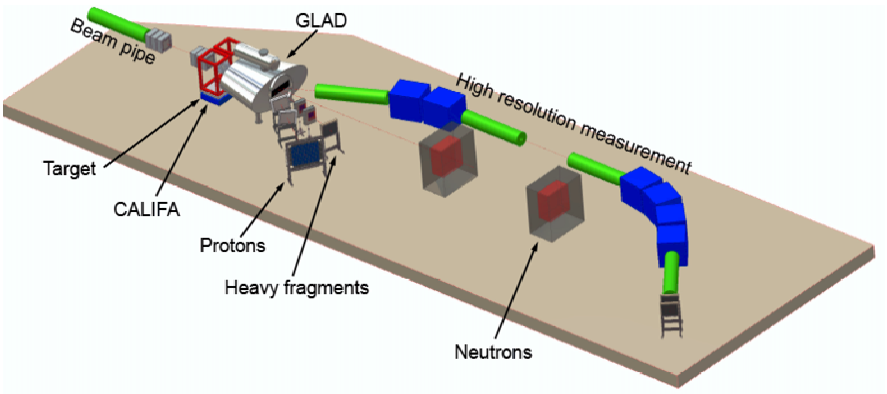

Figure 2: Schematic overview of the R^3B experiment.

with a target, producing a wide variety of lighter nuclei. These nuclei then pass through a fragment separator (known as the Super-FRS) consisting of a series of superconducting dipoles and quadrupoles. Depending on the characteristics of the incident particles, the change in their trajectories resulting from the magnetic fields will vary, allowing only the particles of interest to make it through all of the bends. Thus, a secondary beam, consisting only of the nuclei of interest is produced. The particles of the secondary beam are then collided with another target inside the CALIFA calorimeter, and the scattered particles are detected and measured.

2.2.2 CALIFA scintillator crystals

A scintillator is a material capable of absorbing the deposited energy of an incoming particle through excitation and re-emitting this energy in the form of photons, i.e., as a flash of light. Materials such as organic and inorganic crystals, liquids, glasses, plastics and gases can be used as detector materials. Scintillation in inorganic crystals is an effect of the electronic band structure of these materials. Incoming particles excite electrons from the valence band to the conduction band or exciton band, leading to photon emission when these electrons de-excite. This process can be modified by adding impurities to the crystal which aid in capturing the excited electrons. By coupling a scintillating material to a light-sensitive sensor, like a photomultiplier tube (PMT) or a photodiode (PD), it can be used for particle energy measurements. The materials of interest for the CALIFA detector array are of the type inorganic crystals and include thallium-doped cesium iodine (CsI(Tl)), cerium-doped lanthanum bromide ($LaBr_3$(Ce)) and cerium-doped lanthanum chloride ($LaCl_3$(Ce)).

The CALIFA detector array is planned to consist mainly of CsI(Tl) detectors arranged in a barrel-shaped structure surrounding the beam target, as can be seen in figure 3. CsI(Tl) has already been tested for these applications, and has proven to exhibit suitable characteristics. There is, however, also an end cap on this barrel structure for measuring particles in the for-

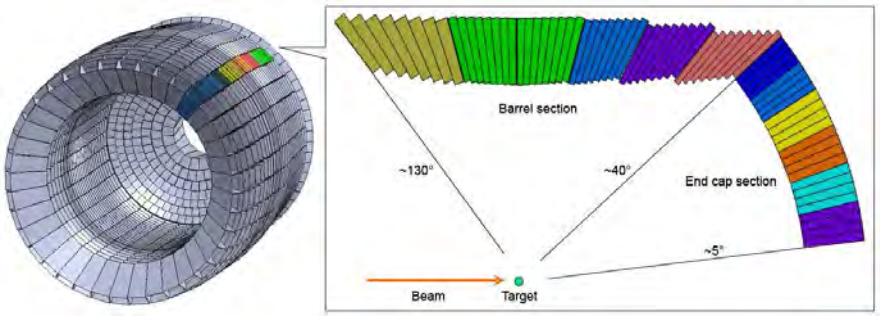

Figure 3: Artistic view and cross-section of the CALIFA calorimeter.

ward direction, in the case of CALIFA, protons and γ photons. As these particles have much higher energies than particles scattered in larger angles from the beam, there are additional considerations to be made regarding the end cap scintillators. Mainly, they will need much larger "stopping power" to prevent the high-energetic particles from completely passing through the material, leading to only a portion of their energy being deposited in the material. The most obvious ways to accomplish this is to either make the scintillators longer, i.e., placing more scintillating material between the target and the sensor, or to use a denser material. However, when also considering the energy resolution, time resolution and, unfortunately, the cost of each scintillator, the situation becomes more complicated.

To solve the problem of measuring highly energetic particles in the forward direction, a couple of different approaches are currently under evaluation. The first option is to use the same kind of CsI(Tl) crystals as in the barrel, only making them longer. The main problem with this approach lies in reaching a sufficient energy and time resolution with these longer crystals. A second option is to use a denser material, the main contestant being $LaBr_3$(Ce). This approach, however, suffers heavily from economic restrictions as $LaBr_3$(Ce) is a relatively expensive material. There are also severe technical challenges in manufacturing suffiently large crystals. To overcome these economic difficulties, a third option has been suggested; a phoswich scintillator consisting of a smaller $LaBr_3$(Ce) crystal attached to a $LaCl_3$(Ce) crystal in a sandwich structure and coupled to a single, common read-out. γ rays would then predominantly interact in either one of the crystals, whereas for charged particles some of the energy would then be deposited in the $LaBr_3$(Ce) and the rest in the cheaper, albeit somewhat inferior, $LaCl_3$(Ce), thus reducing costs while maintaining sufficient time and energy resolution. This approach does however introduce a new problem, namely, how to determine the magnitudes of the different materials' contributions to the measured light emission. Since the two materials have different time and energy characteristics, the measured pulse has to be correctly separated into two components, one for each material, before the particle's energy can accurately be determined.

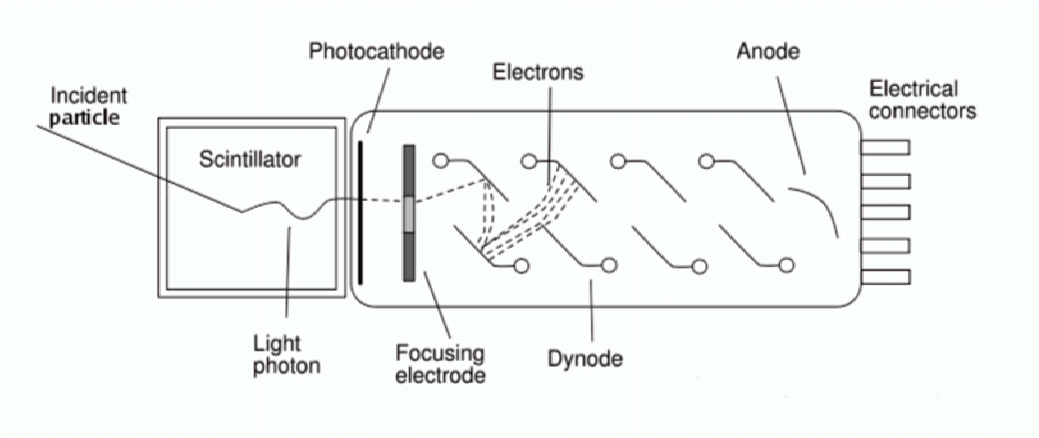

Figure 4: Schematic view of a photomultiplier tube.

2.2.3 Read-out devices

There are three main types of read-out devices used with scintillating crystal detectors; PMTs, PDs and avalanche photodiodes (APDs).

PMTs operate by letting the incident photons strike a photocathode, leading to emission of electrons due to the photoelectric effect, as seen in figure 4. These electrons are then focused and accelerated through a chain of dynodes with an increasing voltage in each step. As the electrons strike each of the dynodes, additional electrons are released leading to a multiplication effect. As the electrons reach the anode of the PMT, the charge produces a sharp current pulse which can then be measured. PMTs provide a high gain, low noise and fast response. However, their sensitivity to magnetic fields is a potential problem when considered for use in CALIFA due to the presence of the GLAD magnet. Another point of consideration is that the gain of PMTs is dependant on both temperature and voltage, thus requiring stable thermal conditions and power supply.

PDs, like regular semiconductor diodes, consist of a PN or PIN junction. When the material is struck by an incident photon of sufficient energy, a mobile hole-electron pair is produced through excitation, producing a photocurrent. Although PDs have proven sufficient for detecting protons and high energy γ photons in CALIFA, their noise level is too high for satisfactory measurements of low energy γ photons.

APDs are structurally similar to regular PDs but operate at a much higher reverse bias. This allows the current carriers to be multiplied by avalanche breakdown, creating an internal gain. Thus, the APD combines properties of the PMT and PD, resulting in sufficient γ resolution without the sensitivity to magnetic fields exhibited by PMTs. However, just like PMTs, the gain of APDs varies with voltage. On top of this, APDs are also highly sensitive to temperature variations.

3 TSL experiment

During March 2009, an experiment was conducted at the The Svedberg laboratory in Uppsala to test the proton energy measurement performance of several types of scintillating detector prototypes for CALIFA. Specifically, the test consisted of a quality control test of CsI crystals as well as a test of a new, somewhat experimental, $LaBr_3$(Ce)-$LaCl_3$(Ce) phoswich detector. This section aims to give a brief description of the experimental setup and the method used throughout the experiment. The main purpose however, is to describe the design and operation of the data acquisition system used throughout the tests.

The general setup of the experiment can be separated into five main parts; beam, detector, pre-processing, data acquisition and data processing. A low-intensity proton beam at 180 MeV was provided by the Gustaf Werner Cyclotron and collimated to provide suitable characteristics. The detector prototypes were then positioned in the beam line behind a double silicon strip detector, providing positional data from the incoming protons. After passing through pre-processing electronics, the detector signals were measured by the DAMs of the DAQ system and measurement data was transmitted over an Ethernet connection for further processing and analysis. Scaler modules were used to provide information on the measurement frequency and the ratio of accepted events to requested events, as well as to aid in debugging the system. For an overview of the experimental setup, refer to figure 5.

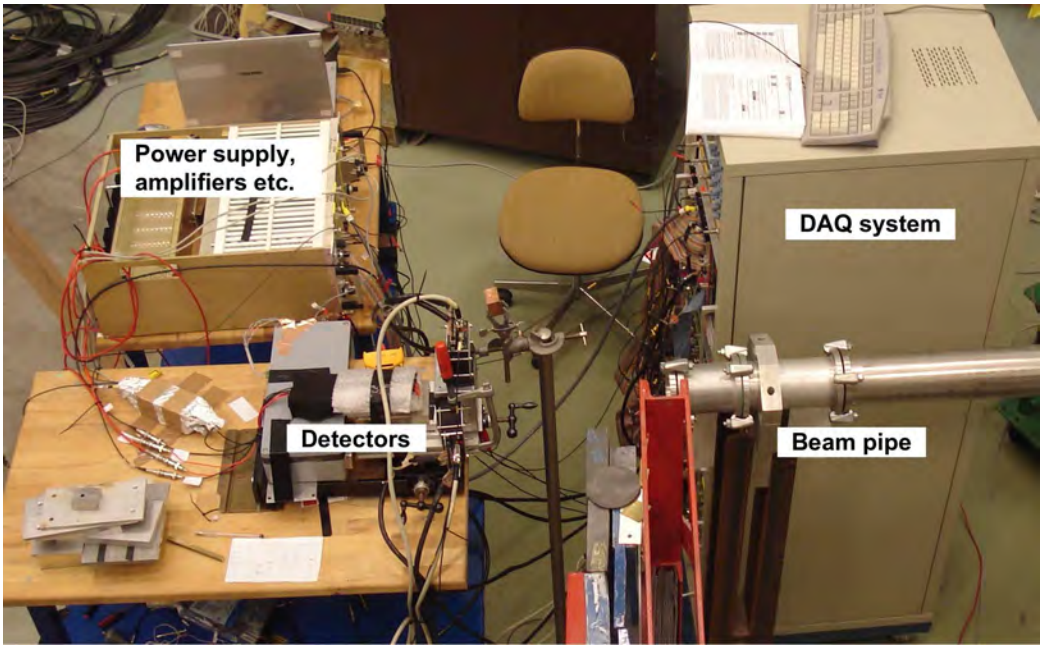

Figure 5: Overview of the TSL experiment setup.

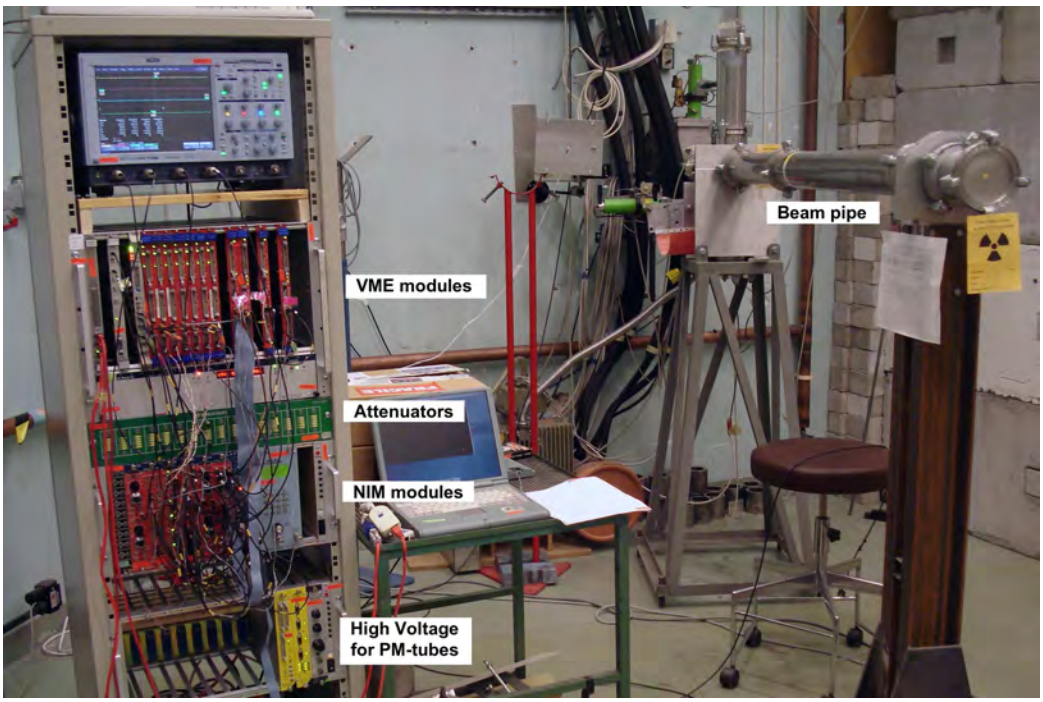

Figure 6: View of the DAQ system and beam pipe. The modules were mounted in several crates, as seen to the left in the picture. The computer to the right of the DAQ was used for monitoring and debugging.

3.1 Data acquisition

The purpose of this section is to briefly describe the experiment setup used for the DAQ system. The concepts of a general DAQ system can be found in A. For the experiment conducted at The Svedberg Laboratory, a data acquisition system based on the NIM and VME standards was assembled, as seen in figure 6. NIM modules were used for control logic, and VME modules were used for data acquisition control and actual measurements. [5]

3.1.1 Experiment DAQ setup

To begin the acquisition of an event, a trigger request is sent from the CFD. For a trigger to be successfully generated several conditions must be met. A FIFO module was used to collect the busy signals from the VME modules and generate a veto signal which in turn was used in conjunction with physics requests from the experiment to control the trigger logic. Also a VME ACQ control card must confirm that the VME modules are ready to be read out. A simple AND/OR logical module was employed for this purpose. The trigger signal was also forwarded to a timer module to generate gates for the acquisition modules and the end markers for the TDC modules. A NIM-ECL translator was employed to collect the signals that were to be measured by the scaler.

A Motorola CPU was used together with an ACQ control card to conduct the VME module programming and read-out, as well as for sending acquired data to storage via a network stream. For the acquisition several CAEN V775 TDCs [6] and V785 ADCs [7] were used for the duration of the experiment, along with V820 scaler modules [8]. For the phoswich measurements an SADC [9] was used to digitize the entire pulses for offline analysis.

3.1.2 Debugging

During the experiment, some issues with the DAQ setup arose. The main issue early on was mismatching of scaler event counts, leading to a full data read-out reset. The nature of the error led to the conclusion that there was too much of a time difference between the triggering of the different modules. Prior to this, the trigger signal was daisy-chained through the DAMs, generating an unnecessarily large time difference between the first and last modules. This problem was solved by distributing individual triggers to the DAMs through a FIFO unit, thus eliminating the time difference.

Towards the end of the experiment another issue was encountered; at times the VME crate would shut down, resulting in lost beam-time and reducing the rate of data acquisition. The initial hypothesis was that there was insufficient power to run the crates, oscilloscopes and other electrical equipment. Therefore, a separate wall socket was tested without success. The next assumption was that the crate power supply was faulty, which, unfortunately, could not be confirmed until after the experiment due to the lack of a backup power supply.

3.2 Phoswich and $LaBr_3$(Ce) tests

The phoswich and $LaBr_3$(Ce) detector tests were carried out during one day of (somewhat sporadic) beam time. Phoswich data was acquired both for the entire detector and for the two different materials individually to enable a full analysis of the detector's characteristics. Due to the design of the phoswich detector, entire pulses had to be digitized, rather than just their amplitudes, in order to provide sufficient information. Thus, SADC modules were used for these tests alongside the regular ADC modules used for testing the CsI(Tl) detectors.

First, data was acquired for the single $LaBr_3$(Ce) crystal placed along the beam direction, i.e., positioned in the same manner as it would be in an actual implementation (configuration 1 in figure 7). The entire phoswich was then tested in the same manner (configuration 2 in figure 7). These tests were performed over several runs, with the detectors' positions and amplification levels being adjusted in between the runs to improve the quality of the acquired data.

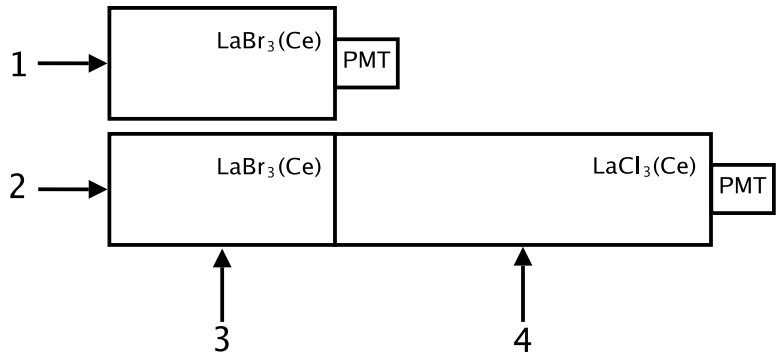

Figure 7: Schematic view of the detector and beam positions during the different runs. Only configuration 2 tests the phoswich as it will be implemented at R^3B.

After these first runs, the $LaBr_3(Ce)$ and $LaCl_3(Ce)$ components of the phoswich were tested individually. These tests were performed by placing the phoswich perpendicularly to the beam line, and with only one of its components in the beam (configurations 3 and 4 in figure 7). During these runs, the single $LaBr_3(Ce)$ crystal was placed behind the phoswich, catching the protons that completely penetrated the phoswich.

Additional data from the full phoswich detector was then acquired using configuration 2 in figure 7, this time with two different beam collimators. The first collimator setting, 20 mm of iron, provided 120 MeV protons, and the second, 25 mm of aluminium with an aperture, provided proton energies of 155 and 180 MeV.

3.3 Data processing

Information recorded by the DAQ system must be transformed from raw data to a readable format, before being analysed in suitable software such as ROOT. In order to extract the raw data, a program called ucesb was employed. With this tool, the data from the DAQ could be recorded and ROOT files containing a tree with information from the DAMs could be generated. The tree contains variables which for each event registered have a corresponding value or sets of values. [11]

3.3.1 Hardware and Networking

To store the data acquired during the experiment, a continuous data stream was transmitted over an Ethernet connection from the DAQ processor. The data stream could then be accessed by any computer on the network. To avoid putting unnecessary strain on the DAQ processor, it was decided to use a second computer an access point for the data stream. To ensure that the data acquired was not lost, a NAS server was constantly connected to this access point, storing the data. For redundancy, the data was also sent to a storage server at Chalmers.

3.3.2 Online analysis

During the measurements, positional data from the silicon strip detectors along with corresponding pulses registered in the SADC were recorded. The positional data was plotted in real-time, and these plots were used for calibrating the position of the beam on the detectors. Also, ROOT was used to draw SADC pulses in real-time to ensure that the recorded data was correct. Hence, the ROOT plot acted as an oscilloscope view, showing the pulses from the detectors due to energy deposition from protons.

4 Data analysis and results

This section aims to present, explain and briefly evaluate the results obtained from analysis of data from the TSL experiment, as well as the methods used to obtain these results. The main concern and focus of the analysis is to separate the energies deposited in the two different materials of the phoswich. The analysis also attempts to verify these results by reconstructing the characteristic phoswich pulses through a linear combination of reference pulses for the two different materials.

4.1 Analysis methods

The main focus of the data analysis is to separate the digitized pulses from the phoswich tests into two components corresponding to the two different materials of the detector. This separation is required if one wishes to obtain a correct measurement of incident particle energies.

The analysis uses digitized pulses from SADCs as well as pre-processed amplitude measurements from regular ADCs. From calibration with protons of a well known energies, the amplitudes measured by these instruments can be converted into well defined energies.

4.1.1 Pile-up

Pile-up events occur due to high event rates or large scintillator timing constants, resulting in several physical events being measured within the same gate. Pile-up events can be classified as tail pile-up or peak pile-up, depending on where the pile-up occurs. In the case of tail pile-up, distinguishable peaks can easily be seen in SADC data and thus considered in the analysis. In the case of peak pile-up however, it can be relatively difficult to distinguish the peaks, as they might look like a single peak, albeit much larger. An example of a tail pile-up can be seen in figure 8.

Pile-up issues can be addressed in various ways. The two most effective ways of eliminating pile-up is by observing data from the silicon strips or the TDCs. If two particles are detected simultaneously in the silicon detector, or the TDC records several events within the same gate, the event should be discarded as pile-up. Shortening the gate is insufficient, as pile-up can occur due to a particle entering the scintillator just before an event has been registered, leading to tail pile-up on the particle that previously entered the scintillator. However, as a part of the calibration process, the beam could be set to low intensities or defocused, so that fewer particles per unit-time enter the scintillator. As pile-up events will always occur, the ability to distinguish those events from the desired ones is crucial for successful analysis results.

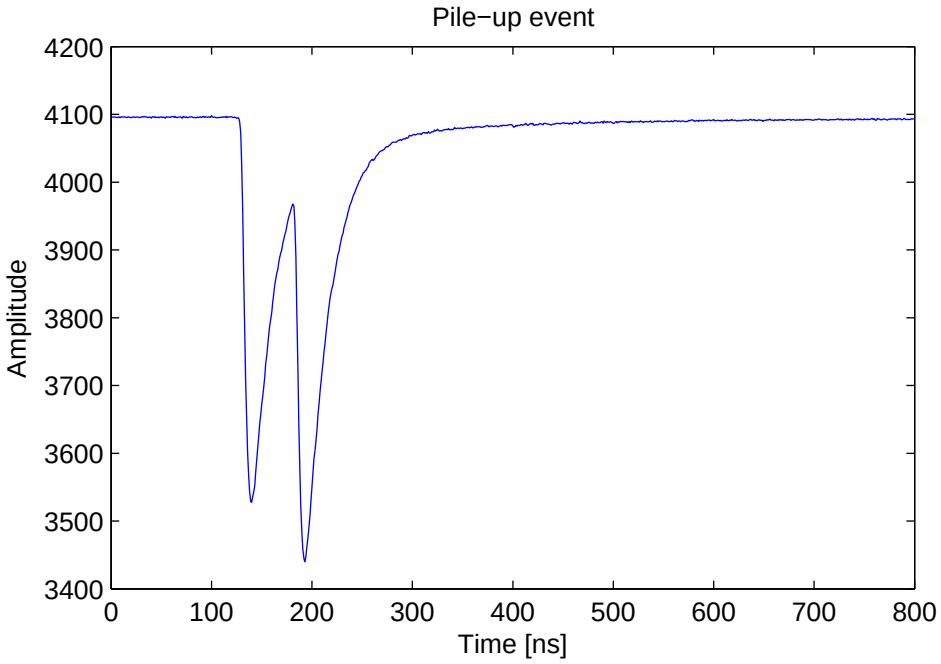

Figure 8: An example of a pile-up event when observed in the SADC data.

4.1.2 Pulse separation

Two different approaches were used for separating the phoswich pulses, using amplitudes and integrals for pulse characterization. These two methods will henceforth be referred to as the *integral method* and the *amplitude method*.

Integral method

The *integral method* [10] separates pulses based on the ratio of the integral over a pulse's tail portion (I_{del}) to the integral over the entire pulse (I_{tot}) as seen in figure 9. This approach is based on the assumption that while I_{tot} is related to the total energy deposition, I_{del} will be related only to the portion of this energy contained within the tail of the pulse. When drawing a scatter plot of these two parameters against each other, pulses with similar ratios, i.e., corresponding to the same type of events, will be observed as straight lines.

Amplitude method

The *amplitude method* utilizes the ratio of the pulses' integrals to their maximum amplitudes for separation into components corresponding to the different materials. The reasoning behind this method is the same as for the *integral method*, assuming instead that a pulse's integral, (I), has a stronger correlation to where the energy has been deposited than its maximum amplitude (A_{tot}). Hence, in an event where all of the incident particle's energy has been deposited in one material, the I to A_{tot} ratio observed should differ from an event where energy has been deposited in the other, or both, materials.

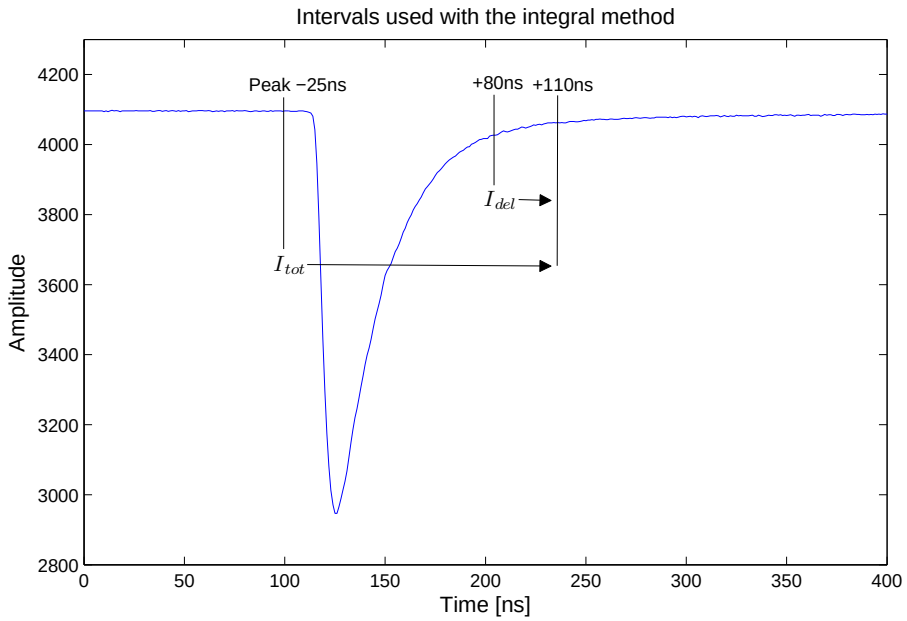

Figure 9: Illustration of the two different intervals used in the *integral method*.

The results acquired using this method should exhibit large similarities to those acquired using the *integral method*. Also, decomposition of pulse amplitudes can be performed in the same manner as for the integrals, resulting in separation of the two amplitude components.

Decomposition of integrals

Based on the *integral method*, detector pulse components will be linearly related according to (6) when considered separately.

$$I_{del}^{Br} = a_{Br} I_{tot}^{Br} \qquad I_{del}^{Cl} = a_{Cl} I_{tot}^{Cl} \tag{6}$$

Where the superscripts Br and Cl refer to $LaBr_3(Ce)$ and $LaCl_3(Ce)$ respectively. Assuming that pulses corresponding to different energies deposited in the same material have the same shape, the coefficients a_{Br} and a_{Cl} will be constants, and due to the different time characteristics of the materials, they will differ from each other. This is a requirement if the pulses are to be separated. When combined pulses, originating from energy deposition in both materials are analysed, it is assumed that the integrals (6) combine into the integrals in (7).

$$\begin{aligned} I_{tot} &= I_{tot}^{Br} + I_{tot}^{Cl} \\ I_{del} &= I_{del}^{Br} + I_{del}^{Cl} = a_{Br} I_{tot}^{Br} + a_{Cl} I_{tot}^{Cl} \end{aligned} \tag{7}$$

The coefficients a_{Br} and a_{Cl} can be determined by identifying events corresponding to energy deposition in only one crystal, thus containing no contribution to the pulse from the other, see section 4.2. Equations (7) then simplify to (8).

$$a_{Br} = \left.\frac{I_{del}}{I_{tot}}\right|_{I_{tot}^{Cl} = 0} \qquad a_{Cl} = \left.\frac{I_{del}}{I_{tot}}\right|_{I_{tot}^{Br} = 0} \tag{8}$$

Thus, (7) is reduced to a system of two equations of two unknown variables, which when solved gives the individual integrals (9).

$$I_{tot}^{Br} = \frac{I_{del} - a_{Cl} I_{tot}}{a_{Br} - a_{Cl}} \qquad I_{tot}^{Cl} = \frac{a_{Br} I_{tot} - I_{del}}{a_{Br} - a_{Cl}} \tag{9}$$

Hence, the relative deposition in the different materials can be obtained.

4.1.3 Energy calibration

Once the integral of a pulse has been separated into its individual components these need to be calibrated in order to obtain the energy deposited in each crystal. The integral of the pulse is proportional to the amplitude obtained from the read-out devices, which in turn, for charged particles, is assumed to be linearly proportional to the deposited energy. This results in a linear system of equations (10), where b_{Br} and b_{Cl} are unknown constants.

$$\begin{aligned} I_{tot}^{Br} &= b_{Br} E_{Br} \\ I_{tot}^{Cl} &= b_{Cl} E_{Cl} \\ E_{tot} &= E_{Br} + E_{Cl} \end{aligned} \tag{10}$$

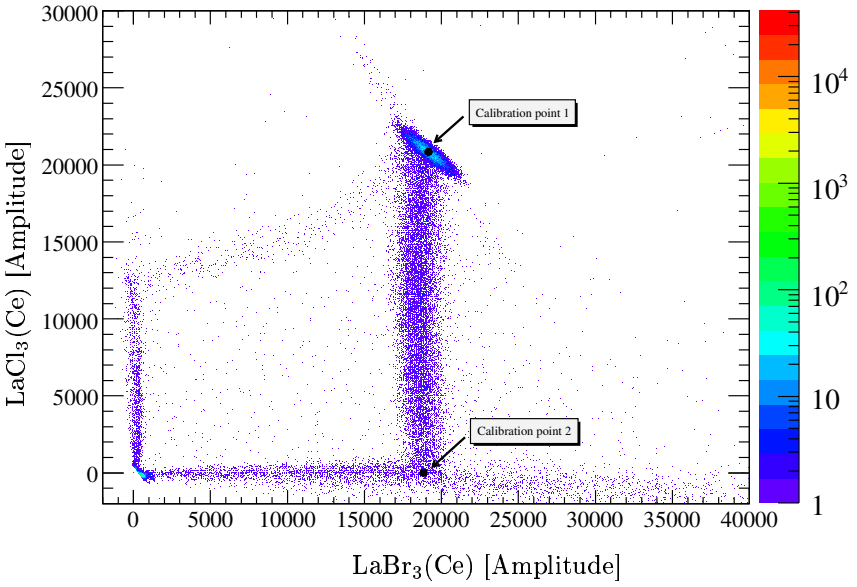

Figure 10: Separated integrals with calibration points.

The solution to (10) is a relationship between b_{Br} and b_{Cl} expressed in the quantities I_{tot}, I_{del} and E_{tot}. This means that two calibration points, for which all three quantities are known, are needed to determine both b_{Br} and b_{Cl} separately. If the indices 1 and 2 refer to these two points, the calibration results in (11).

$$
\begin{aligned}
b_{Br} &= \frac{I^{Cl}_{tot_2} I^{Br}_{tot_1} - I^{Cl}_{tot_1} I^{Br}_{tot_2}}{E_1 I^{Cl}_{tot_2} - E_2 I^{Cl}_{tot_1}} = \frac{I_{tot_2} I_{del_1} - I_{tot_1} I_{del_2}}{E_2 I_{del_1} - E_1 I_{del_2} - a_{Br}(E_2 I_{tot_1} - E_1 I_{tot_2})} \\
b_{Cl} &= \frac{I^{Cl}_{tot_2} I^{Br}_{tot_1} - I^{Cl}_{tot_1} I^{Br}_{tot_2}}{E_1 I^{Cl}_{tot_2} - E_2 I^{Cl}_{tot_1}} = \frac{I_{tot_2} I_{del_1} - I_{tot_1} I_{del_2}}{E_2 I_{del_1} - E_1 I_{del_2} - a_{Cl}(E_2 I_{tot_1} - E_1 I_{tot_2})}
\end{aligned}
$$

Resulting in a relationship between the deposited energies within the different materials of the phoswich.

4.2 Event characterization

As described in section 4.1.2, I_{tot} and I_{del} have been plotted to each other, resulting in a scatter plot where different events can be separated and characterized. Results from 180 MeV phoswich data analysed with the *integral method*, can be seen in figure 11. Each colour in the figure represents a certain type of event, as described below. Also, figure 12 provides a graphical representation of these different event types.
The blue spot corresponds to the complete deposition of the incident proton's energy, since these events have the highest I_{tot} values. Most of the events

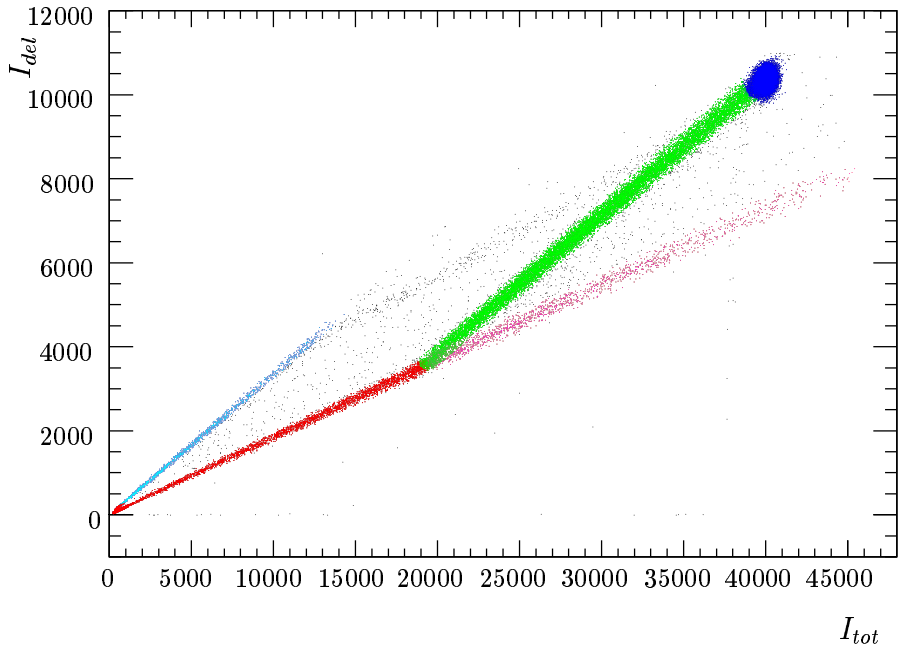

Figure 11: *Integral method* analysed phoswich data from a 180 MeV proton beam. The colours represent events with similar characteristics but different energies.

are also concentrated here, which fits well with the monoenergetic particles striking the detector. These events have large contributions from both the $LaBr_3(Ce)$ and the $LaCl_3(Ce)$ to their measured pulses.

Similar events are represented by the green line, but with smaller integrals implicating a smaller energy deposition. This can be explained by protons scattering out of the detector, resulting in partial energy deposition, or collisions between protons and nuclei leading to neutron emission. As neutrons have a long mean free path within the scintillating material, these events would also lead to only a portion of incident proton's energy being observed. These events will also have contributions to the measured pulse from both the $LaBr_3(Ce)$ and the $LaCl_3(Ce)$.

To determine the origin of the red line, the design of the phoswich has to be considered. These protons first enter the $LaBr_3(Ce)$, depositing a portion of their total energy before exiting the detector or transferring their energy to neutrons. As the deposited energy increases, the events are plotted further up the red line, until the proton enters the $LaCl_3(Ce)$, leading to the combined signals of the green line.

This explains both the sharp "elbow" in the transition from the red to the green line, as well as the magenta coloured events. The elbow marks the beginning of energy deposition in the $LaCl_3(Ce)$, and the different characteristics of the $LaCl_3(Ce)$ lead to a different slope. Events on the magenta line originate from excessive energy deposition in $LaBr_3(Ce)$ due to collisions

between the proton and a nucleus leading to the release of additional particles. If these particles are protons or α particles, their velocities can be much lower than that of the incident proton, leading to a faster deposition of their energies.

The cyan line has the same slope as the green line, but without the contribution from the energy deposition in the $LaBr_3(Ce)$. The conclusion is that the protons have entered directly into the $LaCl_3(Ce)$, either by scattering from the nearby single $LaBr_3(Ce)$ crystal or directly from the beam, depositing energy only in the $LaCl_3(Ce)$.

The black areas are noise and pile-up events. Thus, the plot provides information both on where the protons have deposited their energies, as well as the amount of energy deposited, showing a clear separation between different types of events.

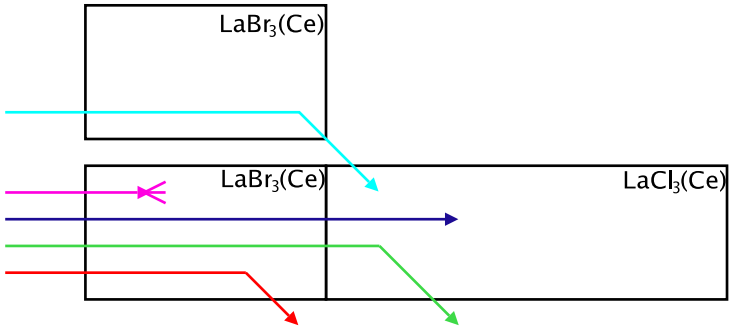

Figure 12: Possible reactions within the experimental crystal setup.

The results of the *integral* and *amplitude methods*, as described in 4.1.2 are shown in figure 13. As expected, the results are similar to those acquired from the *integral method*. However, as can be seen in the figures, the *integral method* provides a better separation of events.

Measurement data from the 155/180 MeV collimated beam run can be seen in figure 14. Because of the two different incident proton energies there are two spots in the figure, corresponding to 180 MeV and 155 MeV protons respectively. The larger I_{tot} values of the events in the rightmost spot indicates that these events correspond to 180 MeV protons.

The validity of this assumption can be verified from the silicon detector data; by selecting events from one spot and plotting the silicon detector data corresponding to these events, the position where these protons have struck the silicon detector can be determined. Figure 15 shows the result for events in the red spot and figure 16 shows the result for the green spot. Observe that the events in figure 15 are more focused than those in figure 16, indicating that these protons went through the small aperture in the collimator, thus having an energy of 180 MeV when reaching the phoswich.

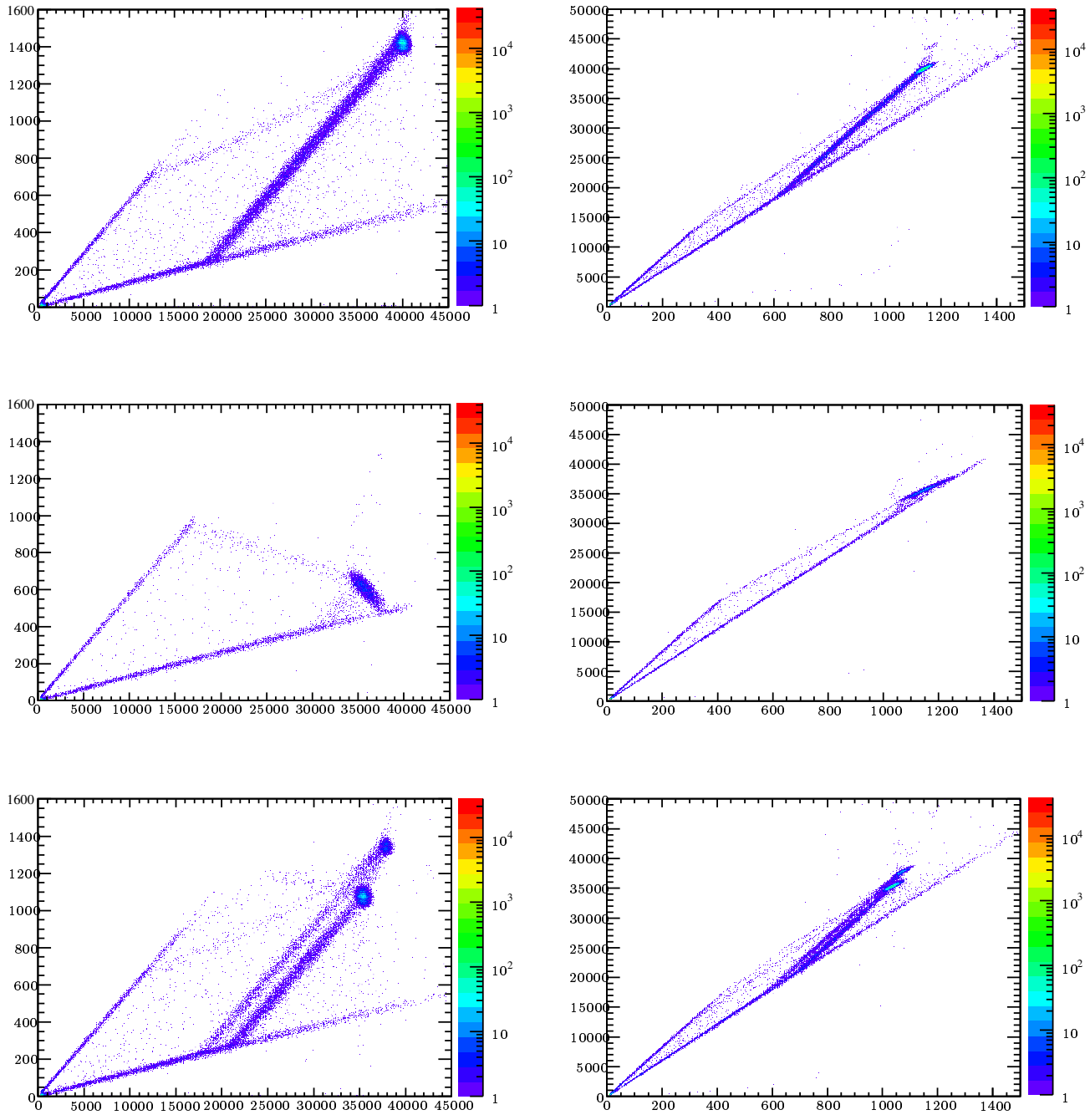

Figure 13: Results from the *integral method* are shown to the left and the *amplitude method* the right. The first four plots represent 180 and 120 MeV respectively and the last two 180 and 155 MeV in one.

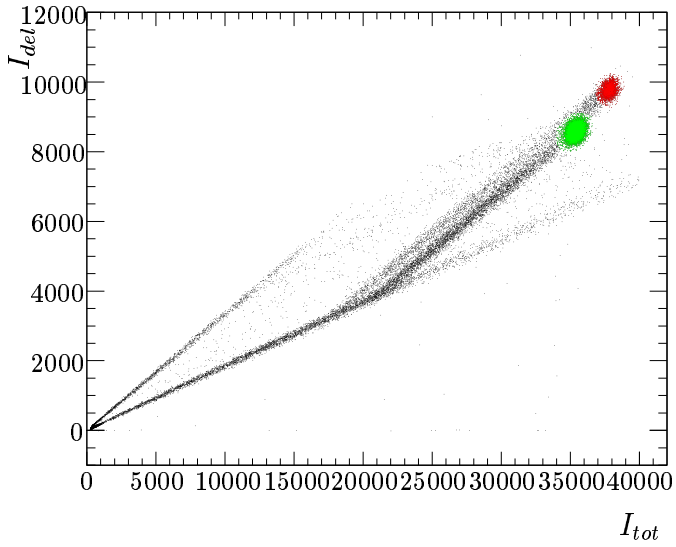

Figure 14: 180 and 155 MeV peaks in the phoswich data.

Also note that the events in figure 15 are aligned more to the left, around position (15, 15), compared to the events in figure 16, which are centered around position (17, 15). This implies that the protons corresponding to the different energies enter the silicon detector at different positions related to the positions where they have struck the collimator. Thus, the events in the red spot in figure 14 is the beam of 180 MeV and the events in the green spot is the beam of 155 MeV.

Another way to ensure that the rightmost spot in the figure is the representation of 180 MeV protons is that this spot lies on the first line diverging from the LaBr-line (events that only deposit energy within the $LaBr_3$(Ce)-crystal). A proton with a higher energy penetrates the first part of the phoswich with less energy loss than a proton with a lower energy, thus causing the higher energy line to diverge from the LaBr-line earlier than the lower energy line.

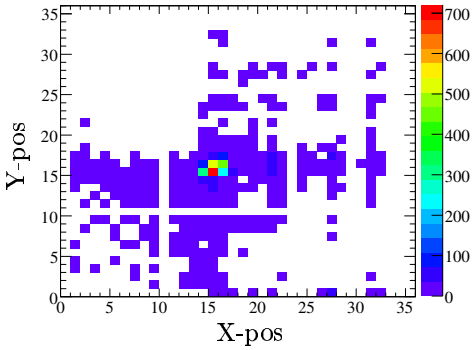

Figure 15: Silicon strip positional data of the 180 MeV proton beam.

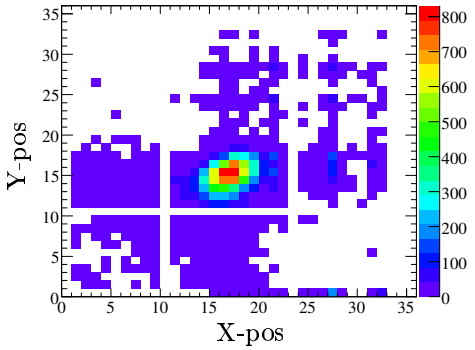

Figure 16: Silicon strip positional data of the 155 MeV proton beam.

4.3 Proton energy determination

The total deposited energy in the phoswich was calculated according to section 4.1, and the following results represent the different tests that were conducted. The experiment data was stored in files according to when it was acquired. These files were named on a serial number basis, e.g. `run_xxx_yyyy`.

Figure 10 on page 19 shows calibration data from `run_060_0002` after I_{tot} has been separated into I_{tot}^{Br} and I_{tot}^{Cl}. Also shown are the points used to calibrate the energy and for which the energy is known. Since this run was performed with 180 MeV protons, the peak and calibration point 1 corresponds to a total energy of 180 MeV. The total energy at point 2 should be 50 MeV, which was the "punch-trough" energy of the $LaBr_3(Ce)$ at 180 MeV according to simulations. This calibration resulted in figure 17 and 18. Data marked with red was obtained using the *integral method* and black using the *amplitude method*. As seen in the figures, the *integral method* gives a better result, since this peak is more focused around 180 MeV.

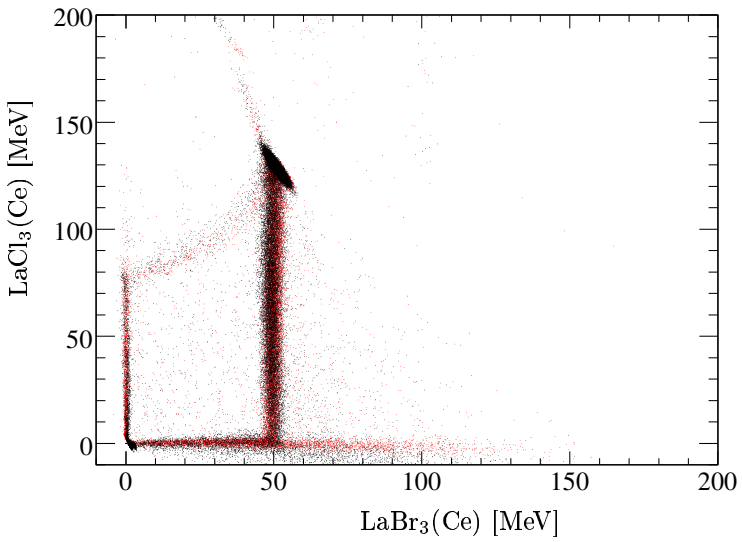

Figure 17: Separated and calibrated energy contributions for the different crystals at 180 MeV.

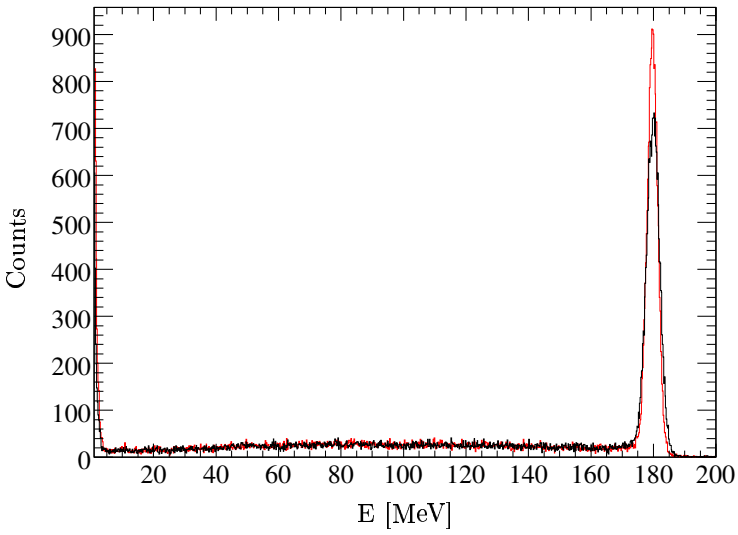

Figure 18: Energy spectrum from 180 MeV protons.

However, this calibration was not sufficient as the instrument settings were changed between runs. The data from `run_070_0001` was re-calibrated using the corresponding calibration points (180 and 50 MeV), the result of which is seen in figures 19 and 20. This run used a collimator, resulting in both 180 and 155 MeV protons, as seen in the figures.

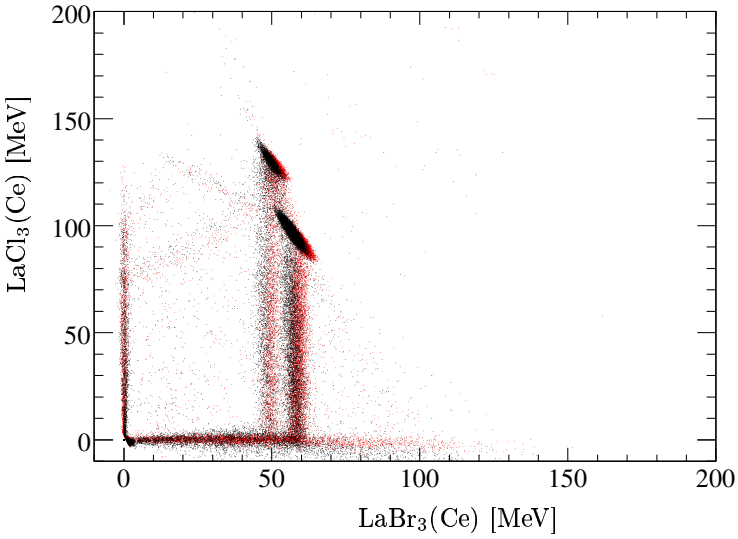

Figure 19: Separated and calibrated energy contributions for the different crystals at 180 and 155 MeV.

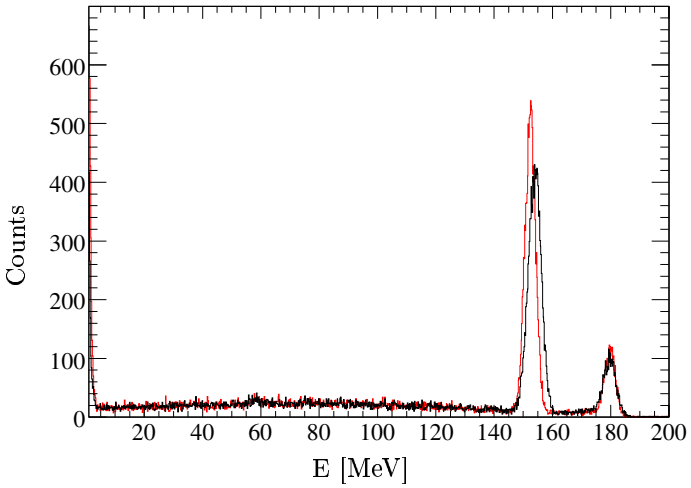

Figure 20: Energy spectrum from 180 and 155 MeV protons.

The energy spectrums shows that the separated energies differ somewhat depending on whether the *integral* or *amplitude method* is used. However, the total energy differs very little, as seen in figure 21. This indicates that both methods deliver good results, although the *integral method* appears to give a better resolution.

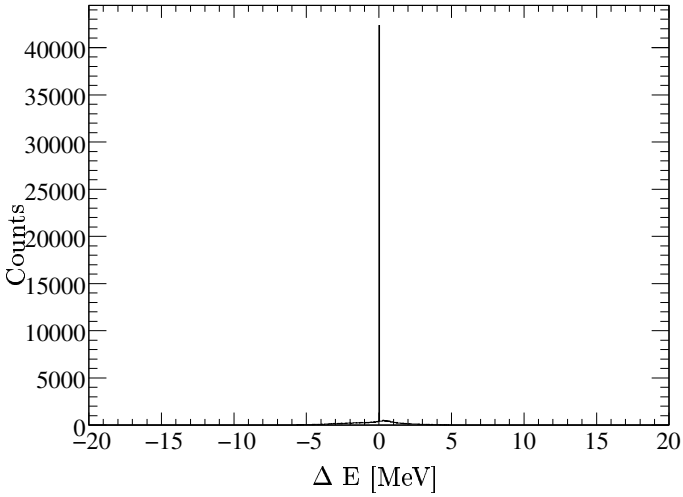

Figure 21: The difference in the total energy for 180 MeV protons, using the *integral* and *amplitude methods*.

4.4 Phoswich pulse reconstruction

To verify the assumption that the combined phoswich pulses are linear combinations of two pulses corresponding to the two different crystals, an attempt was made to recreate the phoswich pulses through combining of two reference pulses. The reference pulses for the two materials were attained using pulse data from the $LaBr_3$(Ce) and $LaCl_3$(Ce) crystals individually, i.e., data acquired using configurations 3 and 4 in figure 7 on page 12. A mathematical function that could be accurately fitted to both the $LaBr_3$(Ce) and $LaCl_3$(Ce) pulses was constructed based on this data. The function described by (11) was found to exhibit properties similar to those of the analysed pulses. A is an amplitude parameter that allows the algorithm to compensate for varying pulse heights.

$$f(x) = \frac{A}{(1 + e^{\frac{x-a_1}{b_1}})(1 + e^{\frac{x-a_2}{b_2}})} \tag{11}$$

To attain correct parameters (a_1, b_1, a_2 and b_2) when fitting the function to the data, empty events and pile-up events had to be discarded. First, empty events were removed from the data set by discarding all events with amplitudes below a specified threshold. Pile-up events were then removed by counting the number of sign changes for the pulses' derivatives above the previously defined threshold, discarding events where this occurred more than once.

The function was then fitted to all accepted pulses from the $LaBr_3$(Ce) and $LaCl_3$(Ce) respectively, saving the parameter values attained for every pulse. After all events in a run had been analysed, the average parameter values were calculated. Thus, two sets of parameters, one for each material, were attained, as shown in table 1 and pulses were reconstructed using (11). The resulting pulses are shown in figure 22.

	$LaBr_3$(Ce)	$LaCl_3$(Ce)
a_1	18.0553	0.4543
b_1	17.9571	29.5326
a_2	23.6815	22.6374
b_2	−1.8757	−1.5380

Table 1: Pulse reconstruction parameters.

A linear combination of the two reference pulse functions, as described by (12), was then fitted with ROOT to the phoswich data (configuration 2 in figure 7) after removing empty events and pile-up in the same manner as described above.

$$\text{Pulse}_{tot} = a \cdot \text{Pulse}_{LaBr} + b \cdot \text{Pulse}_{LaCl} \tag{12}$$

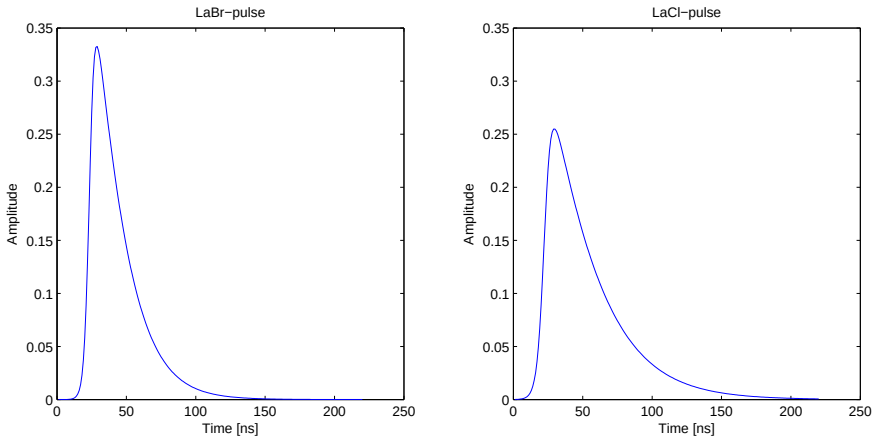

Figure 22: Characteristics of reconstructed pulses, using the calculated parameters for each material.

The relation between the acquired parameter values of this function (a and b) when fitted to the `run_070_0001` phoswich pulses is shown as a scatter plot in figure 23.
The similarity between these results and those obtained using previously described methods, as seen in figure 19, indicates that the assumption made regarding the composition of the phoswich pulses is indeed correct.

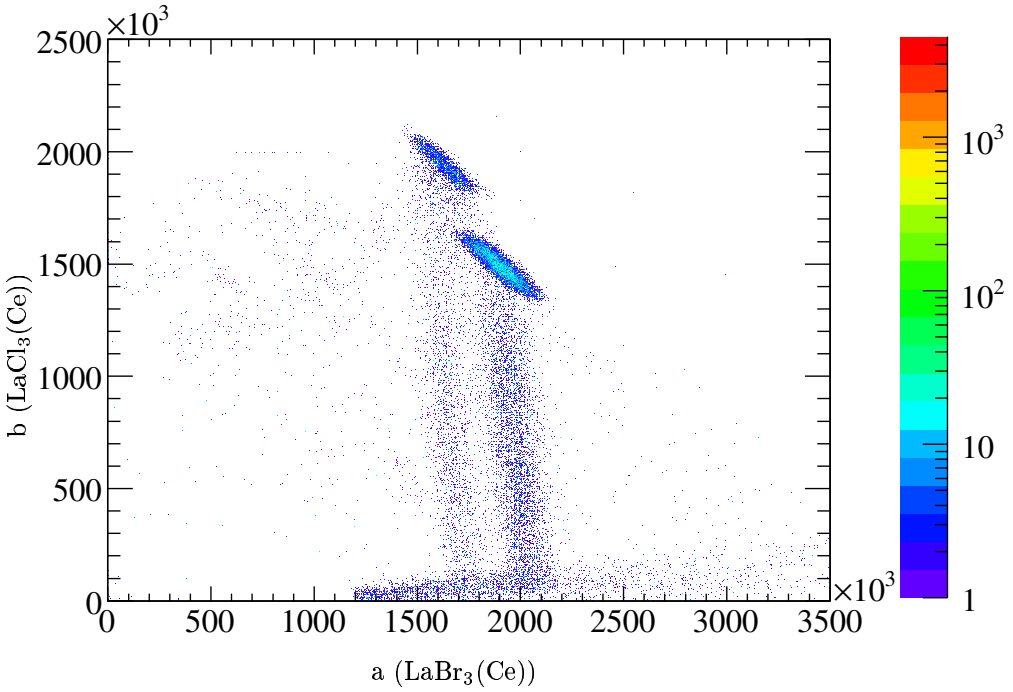

Figure 23: Scatter plot of the fitted parameters a and b.

5 Discussion

This section aims to evaluate the conduction of the TSL experiment, as well as the methods used during the analysis of acquired data.

5.1 Experiment

Overall, the proton beam tests at TSL went quite well. Sufficient amounts of data were acquired for all detector prototypes, and offline analysis indicates that the data acquired is, generally, of sufficient quality.

There were a few issues with the DAQ system, as described in section 3.1.2. However, the only problem that could not be solved was the failure of the VME crate's power supply during the last day of testing. In hindsight, bringing a second backup supply would seem like a good idea. It should however be noted that the crate had been tested at Chalmers before the experiment. This, along with the fact that the crate worked well during the first three days of testing, indicates that this particular problem could not have been predicted. Thus, bringing a second crate was omitted for logistical reasons. Information regarding the detectors and their positioning, collimator settings, amplification levels etc. used in the different runs of the experiment was written in a log. Although this information has been very useful for the data analysis, a more rigorous logging of the experiment would have been beneficial. Making one person responsible for the experiment log might have helped in ensuring that sufficient information was provided for each experiment run.

5.2 Data analysis

Results from the data analysis indicate a clear difference between phoswich pulses corresponding to different types of events. A good separation was acquired both using the *amplitude method* and the *integral method*. The *integral method* required some optimization to determine the best interval over which to calculate I_{del}. This interval could be chosen quite freely and still produce separation, but the best results were acquired using the interval shown in figure 9 on page 17. The shapes of the lines in the *integral* and *amplitude method* figures give a strong indication that the assumption of linearity made during the analysis was largely correct. It should be noted that the methods used are very simple in terms of computation, which means that they should be relatively easy to implement in hardware if one wishes, or to be used in online analysis software. It is important to note that to be able use the methods applied throughout this thesis, either the total energy deposition must be known for two *integral method* separated data points, or the energy deposition in each of the crystals.

6 Conclusion

A well functioning DAQ system for equipment and concept testing was assembled in Göteborg prior to the prototype tests at TSL. A similar system was then assembled and successfully used during the beam tests. The measurements at TSL were conducted without any major issues, and the minor problems encountered were successfully managed.

Analysis of the acquired digitized phoswich pulses indicates that the phoswich pulses can be separated into components corresponding to the two different materials using relatively simple calculations. By separating the measured pulses into these two components, correct proton energies could be extracted from the acquired data. Thus, the phoswich detector appears to exhibit the required characteristics for making good proton energy measurements.

References

[1] Institute of Research into the Fundamental Laws of the Universe, 2007. *Reaction studies with Relativistic Radioactive Beams.* [Online] (Updated 2007-09-21) Available at:
`http://irfu.cea.fr/en/Phocea/Vie_des_labos/Ast/ast_technique.php?id_ast=2108`
[Accessed 2009-02-11]

[2] Alvarez, H., Benlliure, J., Casarejos, E., Cortina, D., Duran, I., Gaseon, M., 2007. *R & D on scintillating crystals for the R^3B Calorimeter.* IEEE Science Symposium Conference Record.

[3] Krane, K.S., 1988. *Introductory nuclear physics.* 2nd ed. United States: John Wiley & Sons.

[4] FAIR/NUSTAR/R^3B, 2008. *Technical status report for CALIFA: The R^3B Calorimeter for Photons and High Energy Charged Particles.* 2008-11-17 ed.

[5] Johansson, H., 2007. *The DAQ always runs - Performing large scale nuclear physics experiments.* Sweden, Göteborg: Chalmers University of Technology.

[6] CAEN Tools for Discovery, 2004. *Technical Information Manual: Mod. V775. 32 Channel Multievent TDC.* Revision 5

[7] CAEN Tools for Discovery, 2003. *Technical Information Manual: Mod 785. 32/16 Channel peak sensing ADCs.* Revision 10.

[8] CAEN Tools for Discovery, 2002. *Technical Information Manual: Mod V820. 32 Channel latching scalers.* Revision 3.

[9] Delagnes, E., Breton, D., 2006. *Documentation of the MATACQ32 board.* Revision 1.8.

[10] Guerro, C., Cano-Ott, D., 2008. *Analysis of the BC501A neutron detector signals using the true pulse shape.* Nuclear Instruments and Methods in Physics Research A, 597 (2008), p. 212-218.

[11] Johansson, H., 2008. *The ucesb unpacker generator, Long write-up - documentation and manual.* Sweden, Göteborg: Chalmers University of Technology. [Online] (Updated: 2008) Available at:
`http://fy.chalmers.se/~f96hajo/ucesb/`
[Accessed 2009-05-13]

A DAQ design and construction

Successful subatomic physics experiments depend on reliable data acquisition systems. The purpose of this appendix is to provide an overview on the design and implementation aspects of such a system. It introduces the general concept and principles for scintillating crystal electronics and data collection, before moving on to the system specific components and its structure. Descriptions of the technical terms and abbreviations may be found in the glossary on page 43.

A.1 DAQ system overview

A general design for data acquisition systems used in subatomic physics experiments can be seen in figure A1. Even more simplified, one could think of this scheme as Detector → Logic → Acquisition. Such a description might, however, not be very useful. Instead, the user will need to have at least a certain amount of knowledge about the common types of modules used in nuclear physics experiments in order to fully benefit from this section.

Figure A1 shows an overview of the functions that must be present in a general DAQ system. In practice, the functions of this system must be realized in terms of actual electronics and wiring, and the problems that this presents must be solved.

Below follows a brief introduction to the three main components of a DAQ system, shown as boxes in figure A1. Box I symbolizes the detector and components that translate physical events into something that can be properly measured by the electronics. This includes amplifiers, filters and cables. Box II represents the system's logical components that determine whether an event can, and should, be handled or not. An important feature of the DAQ system is the dead-time generation, which prevents new signals from interrupting or interfering with the events currently being processed. The frequency of physical events may very well be higher than the maximum frequency at which the DAQ system can read out and store these events. Hence, Box II acts as security, making sure no collected events are overwritten by, or overlaid with, data from another event. Box III contains the actual data acquisition modules (DAMs), such as ADCs and SADCs.

Box I

The signals from the detector are split in order to provide an unharmed analog signal for ADCs/QDCs/SADCs as well as to issue a logical signal from the CFD to the TDCs and the logics in Box II. Due to the latency of the Box II logics, usually a few hundred nanoseconds, the signals sent to Box III must be delayed long enough for the logics to decide whether the detector signals constitute an event to be measured, and whether or not that event can be processed by the DAQ system.

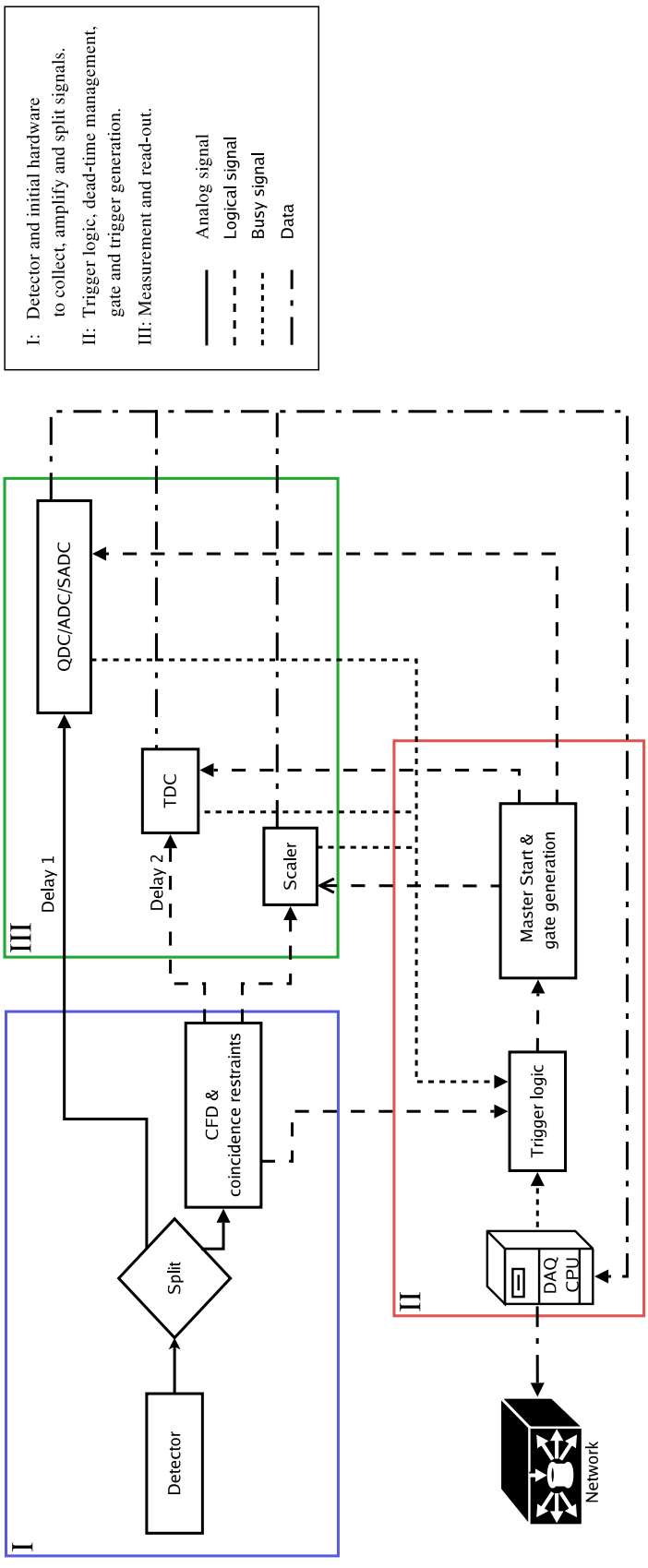

Figure A1: Flowchart of the functions present in a general data acquisition system (DAQ). The delays are necessary to allow the trigger logics to produce gates before the signals reach the DAMs.

The CFD acts as a simple amplitude filter; it determines whether the continuous signal from the detector is larger than a pre-set threshold value (i.e., whether or not the signal contains any interesting information). Hence, it is the DAQ system's first approach in filtering out unwanted noise.

Box II

Once a signal passes through the CFD, a request in the form of a logical pulse is sent to the system's trigger logic. The trigger logic's purpose is to decide if the event is considered to be of any interest and whether or not the system is capable of handling it. As the momentary rate of physical events may very well be higher than the maximum frequency at which the DAQ system can read and store events, this feature, known as dead-time generation, is a very important feature of a DAQ system. Without this, there is nothing to stop new events from interrupting and interfering with the processing of a previous event, making the collected data much more difficult to analyse, if not rendered completely useless. When an event has successfully passed through the trigger logic, gates and trigger signals are generated and forwarded to the DAMs of Box III.

Box III

The components in Box III are responsible for the actual measurement of incoming signals. When an event has been accepted by the logic circuits of Box II, the modules of Box III will be given gate and trigger signals and the actual recording begins. The delays 1 and 2 in figure A1 exist in order to give the trigger logic enough time to generate these gate and trigger signals before the signals from the detectors reach the DAMs. Should this delay be omitted, or calibrated badly, the gates and triggers would not coincide with the actual event data reaching these modules, leading to noise or other unwanted data being measured instead of the requested pulses. Hence, correct calibrations of these delays are crucial to the quality of the collected data.

After an event has been measured, a DAQ processor reads the stored values from the DAMs and transmits the raw measurement data over a network connection for storage and further processing. [1]

A.2 Implementation of DAQ logic

This section gives a description of how the systems trigger logic can be designed in terms of actual hardware and electronics (more specifically; NIM-modules). The trigger logic is crucial to the DAQ and thus need careful explanation and understanding. Once the basic principles described here have been fully understood, one should be able to implement more complex systems with relative ease.

When an event has been accepted by the CFDs, and eventual coincidence restraints are fulfilled, a logical signal called *trigger request* is sent to the input of an AND gate in a logic unit along with an *ACQ on* signal from the

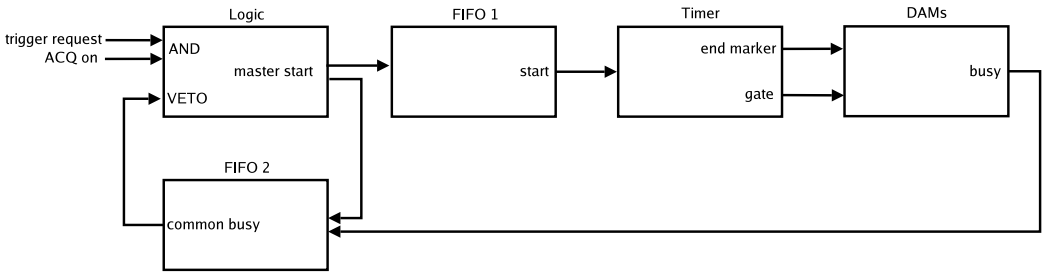

Figure A2: Illustration of DAQ logic implementation.

ACQ controller. This unit is the actual trigger logic of the DAQ system. Its output, a *master start* signal, is sent to a FIFO module distributing *start* signals to the rest of the system. The logic module's veto input is connected to the *common busy*, which disables the generation of *master start* signals when active. Thus, when the trigger logic receives a *trigger request*, a *master start* is only generated if the *ACQ on* signal is active and there is no *common busy* signal. Refer to figure A2 for a signal scheme and clearer view of the components.

The *common busy* signal is acquired from one or several FIFO units that collect *busy* signals from all of the DAM modules. In addition to the *busy* signals, the common busy also includes the *master start* signal from the trigger logic in order to ensure rapid start of dead-time (more on this in section A.3.3).

Start signals are derived from the *master start* and distributed by a FIFO-unit. They are used for generating *gates* and, if one wishes, to trigger scalers in order to provide a count of accepted events. *Gate* and *common start/stop* signals are provided by timer units triggered by the *start* signals.
To summarize; the minimum required units are:

- FIFO 1:
  Input: *Master start*
  Output: *Start*

- FIFO 2:
  Input: DAM *busy* and *master start*
  Output: *Common busy*

- Logic:
  Input: *Trigger request*, *common busy*, *ACQ on*
  Output: *Master start*

- Timer:
  Input: *Start*
  Output: *Gate*, *common start/stop*

Note that one physical module may contain several units, thus saving space.

A.3 Important considerations

This section aims to describe considerations that should be made to ensure a well performing data acquisition system.

A.3.1 Single-event / Multi-event

The DAMs have very limited data buffers, which have to be kept from filling up in order to ensure proper event matching. Measurement data from DAMs can be collected by the DAQ processor in two different ways; single-event mode or multi-event mode. When operating in single-event mode, the DAQ processor will collect data from all of the DAMs after every single event. While performing the read-out, the dead-time is activated to ensure that no new events are measured before the read-out is complete. Event matching of the data becomes trivial when the DAQ system runs in single-event mode, as the data is collected one event at a time, retrieving the event data from every module before the dead-time is released. In general, the speed at which the DAQ processor can collect data is higher than the speed at which DAMs can store data in their buffers. This makes multi-event acquisition possible, providing higher data acquisition rates than with single-event acquisition. When operating in multi-event mode, the modules' buffers are emptied one module at a time, rather than one event at a time. As long as the read-out capacity of the DAQ processor is sufficiently high, this can be performed continuously, without dead-time locking. However, when operating in multi-event mode, event mixing is a potential problem. A well working approach for detecting and minimizing the damage caused by event mixing is to regularly check the event counters of the DAMs, making sure they have counted the same number of events since the last time they were controlled. Thus, if a difference in event counts is detected, only the data collected since the last check is subjected to event mismatching. The dead-time should be enabled while this task is performed.

A.3.2 Pedestal measurements

In order to be able to translate the arbitrary amplitudes measured by the DAMs into particle energies, one must first subtract the background noise level. Determination of the noise level can be done through pedestal measurements triggered by the DAQ processor's ACQ controller. When such an event is triggered, the DAQ system acquires an empty event and measures its amplitude, thus acquiring the amplitude of the background noise. In the case where an event occurs during a pedestal measurement, the measurement is discarded if it exceeds a pre-defined maximum noise amplitude. As the level of noise can drift quite significantly with time, these events should be triggered regularly to ensure accurate noise levels throughout the measurements, and should subsequently only be used in conjunction with the last events.

A.3.3 Rapid start of dead-time

Whichever circuitry and components that are used to realize the DAQ system, correct gate generation, triggering and dead-time locking is vital for the system to work well and produce high quality data. Conceptually, in order to prevent two CFD requests to be handled at the same time, one would wire all busy signals to the trigger logic veto. This is necessary to not allow any event before processing of the previous one is complete.

However, the propagation delays usually make the busy signal become active too late to veto all secondary triggers. During the time it takes for the trigger signal to leave the trigger logic component, until the dead-time veto is activated, the CFD might send yet another physics request. Unhandled, it would overlay and ruin all data currently being processed.

Therefore, the master start signal coming from the trigger logic unit is connected to the trigger logic's veto input, in order to start the dead-time as quickly as possible. However, in more advanced trigger-coincidences, a window of pre-determined length has to be left open. In other words, the system would be "vulnerable" for a pre-determined time. If that is the case, the master start must be set up in such a way that it disables re-triggering during this window, which is achieved by making the signal longer than the latency of the trigger logic and gate generation. For an illustration of these concepts, refer to figure A3.

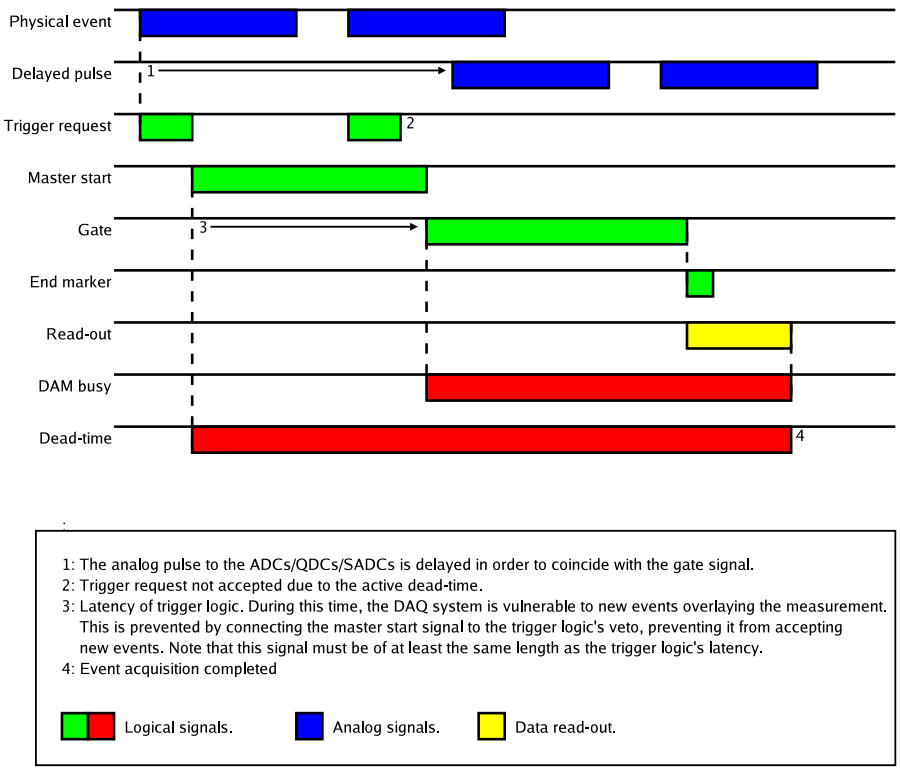

Figure A3: Illustration of dead-time, trigger and gate timing.

A.4 Example: A simple DAQ system

This section gives an example of how a basic DAQ system can be implemented. The example used is the system set up in Göteborg for equipment testing prior to the TSL experiment.

The DAQ system consists of several NIM and VME modules, with a CFD as the link to the detectors. The CFD continuously reads the raw (but possibly filtered and amplified) signal from the detectors and generate trigger signals when the specified conditions are met. These trigger requests are sent to the third sub module of the 3-fold logic unit (which is the systems main trigger logic component) as well as to a scaler via a NIM-ECL translator to provide a count of trigger requests.

The ACQ controller is the interface of the DAQ processor and enables communication between the DAQ software and the system components. The ACQ controller sends an inverted busy signal when the DAQ processor is capable of handling events, which is a requirement for the trigger logic to generate master start signals. It can also issue trigger requests for pedestal measurements.

Whenever the trigger logic (the AND-part of the 3-fold logic unit) receives a trigger request, either from the experiment or the DAQ's ACQ controller, and is not already vetoed by a busy signal, it accepts the trigger and issues the master start signal. In turn, the master start signal is sent to the dual timer for generation of gate signals for ADCs/SADCs and common start/stop signals for TDCs.

The other two modules, the FIFO and NIM-ECL translator, are more or less part of the wiring. They only contribute by adding, splitting or converting signals into suitable formats.

The rest of the electronics perform the actual measurements, their types depending on the experiment. The number of included modules may vary in order to handle any number of channels or preferences. Extra TDCs might be added for timing, ADCs and SADCs for measuring amplitudes. Also, the length of the gate and end markers must be calibrated to suit the specific detector, but the function and operation remains the same. [2, 3, 4, 5]

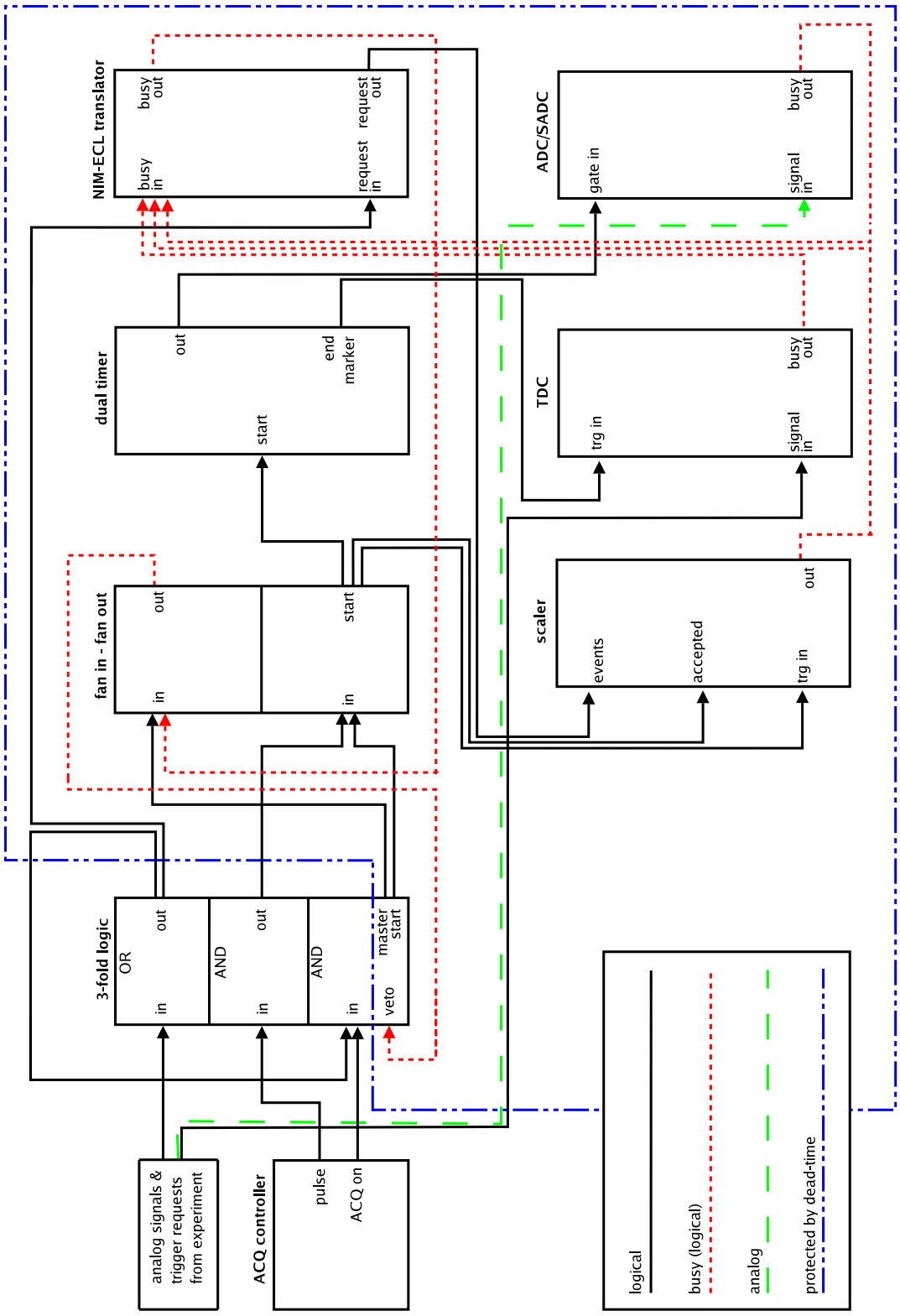

Figure A4: Schematic of the DAQ system used for equipment and concept testing prior to the TSL experiment.

References

[1] Johansson, H., 2007. *The DAQ always runs - Performing large scale nuclear physics experiments.* Sweden, Göteborg: Chalmers University of Technology.

[2] CAEN Tools for Discovery, 2004. *Technical Information Manual: Mod. V775. 32 Channel Multievent TDC.* Revision 5

[3] CAEN Tools for Discovery, 2003. *Technical Information Manual: Mod 785. 32/16 Channel peak sensing ADCs.* Revision 10.

[4] Delagnes, E., Breton, D., 2006. *Documentation of the MATACQ32 board.* Revision 1.8.

[5] CAEN Tools for Discovery, 2002. *Technical Information Manual: Mod V820. 32 Channel latching scalers.* Revision 3.

B Glossary

ACQ Controller - Interface between the DAQ processor and NIM modules. Used for pedestal measurements and in trigger generation.

ADC - Amplitude-to-digital converter. Measures the maximum amplitude of a signal during a gate. Commonly used for silicon diode detectors.

APD - Avalanche Photodiode. A semiconductor based light sensor utilizing avalanche breakdown for signal amplification

CALIFA - A Calorimeter for in-flight emitted gammas and light charged-particles. Calorimeter used in the R^3B experiment for γ and proton energy measurements.

Calorimeter - A device that measures the energy from some physical event. In this case, a device that measure the energy of particles.

CFD - Constant fraction discriminator. Converts analog pulses with amplitudes above a specified threshold into logical signals. The timing of the signal is independent of the pulse height.

DAM - Digital acquisition module. Common term for TDCs, ADCs etc.

DAQ - Data acquisition. Can refer to only the module controlling the data read-out (DAQ processor), its software (DAQ program), or to the entire data acquisition system (DAQ system).

Dead-time - Time during which an event cannot be accepted due to one or more parts of the DAQ being busy, often processing a previous event.

Event - The occurrence of each ion passing through the setup, generating data from the detectors.

FAIR - Facility for antiproton and ion research. Planned facility that will be an expansion of GSI.

FIFO - Fan in-fan out. A NIM module that collects several inputs and distributes the signal to several outputs.

FRS - Fragment separator. Used to focus and separate products after collisions between beam targets and relativistic ion beams.

Gate - Signal during which the inputs of a DAM are open. Usually derived from a common start/stop signal.

GLAD - GSI Large acceptance dipole in the R^3B experiment. Magnet that separates and bends the different particles in directions where the proper detectors are located.

GSI - Gesellschaft für Schwerionenforschung. A facility for ion research located in Darmstadt, Germany.

NAS - Network Attached Storage. A simple file server.

NIM - Nuclear instrument module. A mechanical and electrical standard for the construction of experimental electronics.

Online analysis - A, generally simple, analysis of data in real-time during while the experiment runs. Used for calibration and monitoring.

Offline analysis - Analysis of stored data from an experiment. Generally utilizes more advanced methods than online analysis, requiring more time and computational power.

PD - Photodiode. A semiconductor based light sensor.

Phoswich - A detector composed of two different scintillating crystals in a sandwich-like junction.

Pile-up - Undesirable effect originating from multiple events being measured within the same gate, leading to the output containing a superposition of signals.

PIN-junction - Junction formed by combining P- and N- type semiconductors with a near intrinsic semiconductor region between them.

PMT - Photo-multiplier tube. Measures photons by conversion to electrons, which are then amplified through multiplication.

PN-junction - Junction formed by combining P- and N- type semiconductors

ROOT - A C++ oriented analysis tool, commonly used in subatomic physics experiments.

R^3B - Reaction studies with relativistic radioactive beams. An experiment setup at FAIR.

SADC - Sampling ADC. Samples pulse information at a much higher rate than an ordinary ADC in order to reconstruct and discretisize a signal.

Scaler - Counts the number of logical pulses. Used to determine how often a detector channel or other signal fires.

Scintillator - A material that emits photons after being excited by a passing particle.

Super FRS - A FRS at FAIR.

TDC - Time-to-digital converter. Measures the time between a common start or stop signal and the individual detector signals.

Trigger - Logical signal from the DAQ trigger logic to the DAMs. Determines that a new event can, and should, be processed.

Trigger logic - Part of the experimental electronics that, based on fast coincidences from the detectors, decides when an event has happened and if it should be recorded. Also handles dead-time blocking.

TSL - The Svedberg Laboratory in Uppsala, Sweden.

ucesb - unpack & check every single bit. Software for checking and converting raw measurement data. Can be used for generating ROOT-compatible n-tuples.

VME - A data bus commonly used in industry for computing and control applications.